

AN INVESTIGATION OF ANGULAR STIFFNESS AND DAMPING COEFFICIENTS OF
AN AXIAL SPLINE COUPLING IN HIGH-SPEED ROTATING MACHINERY

C.-P. Roger Ku and James F. Walton, Jr.
Mechanical Technology Incorporated
Latham, New York

and

Jorgen W. Lund
The Technical University of Denmark
Lyngby, Denmark

5/6 = 37
12860
P- 11

ABSTRACT

This paper provided the first opportunity to quantify the angular stiffness and equivalent viscous damping coefficients of an axial spline coupling used in high-speed turbomachinery. A unique test methodology and data reduction procedures were developed. The bending moments and angular deflections transmitted across an axial spline coupling were measured while a non-rotating shaft was excited by an external shaker. A rotordynamics computer program was used to simulate the test conditions and to correlate the angular stiffness and damping coefficients. In addition, sensitivity analyses were performed to show that the accuracy of the dynamic coefficients do not rely on the accuracy of the data reduction procedures.

INTRODUCTION

Internal friction as a problem in rotor-bearing systems was first recognized in the mid-1920s when manufacturers began shrinking disks onto supercritical rotors. Newkirk [1] observed that at speeds above the first critical speed, the rotor would enter into a violent whirling in which the rotor centerline precessed at a rate equal to the first critical speed. Kimball [2] suggested that internal shaft friction could be responsible for the whirling. Since then, numerous contributors [3-6] have provided additional insight into the effects of internal friction.

Today, with the increased power densities of advanced turbopumps and the resultant increased rotor flexibility, internal friction is seen to be a potential source of problems. Turbopumps such as the Space Shuttle Main Engine (SSME) High-Pressure Oxidizer Turbopump (HPOTP) are of built-up design with many joints, fits and areas for friction-induced excitation if slippage takes place. These rotors operate above flexible bending critical speeds and the forces on the rotors are very large, which tends to encourage joint slippage and friction force generation. The rotor instability resulting from this type of vibration is usually cured by adding special dampers, redesigning rotor fits, or modifying the bearings, which does not allow the development of a true understanding of the mechanisms of internal friction. In addition, the practicing design engineer finds very little readily available information on how to model the various couplings which make up the complete rotor system. Often, a rotordynamicist must make an intelligent guess on the dynamic properties of the coupling in order to perform the analysis.

In the design charts of flanged and curvic couplings provided by Bannister [7], flexural stiffness values were provided but no damping data were available. Marmol et. al. [8] developed a

mathematical model to predict the lateral and angular stiffness and damping coefficients of spline couplings. Based on these coefficients, they calculated the natural frequencies of a rotor system and compared them to the experimental data. Recently, Walton et. al. [9] developed three nonlinear analytical models representing interference fits and axial and curvic spline couplings, and integrated them with a transient rotordynamics computer program analysis. Results from this work show the predictability of rotor system instability due to internal friction, which has been experimentally observed, especially for axial splines.

It has been shown that measuring only the natural frequencies of a rotor system cannot accurately verify models predicting angular stiffness and damping coefficients of axial spline couplings [10]. However, no direct measurement has been reported, such as measuring the angular displacement and moment. This paper describe a unique test methodology and data reduction procedures that have been developed determining the angular stiffness and damping coefficients of an axial spline coupling. The bending moments and angular deflections transmitted across the axial spline coupling were measured while a non-rotating shaft was excited by an external shaker. The angular stiffness and equivalent viscous damping coefficient were determined by the interactive use of rotordynamics computer program simulations and experimental measurements. In addition, sensitivity analyses were performed to demonstrate that the accuracy of the data reduction procedures does not affect the accuracy of the results.

EXPERIMENTAL TEST SETUP

The test facility was built to simulate an SSME HPOTP preburner spline. Figure 1 shows the overall test setup and Figure 2 is a functional block diagram of the test setup. The shaft consists of two offset male axial splines and an external female spline sleeve. The shaft was excited by an external dynamic force which was driven by an MTS hydraulic force control system in the X-direction (horizontal). An external damper was installed but was not active while the bending moment and angular deflection were measured. The damper was used to limit the shaft orbit while the system was traveling through its unstable natural frequencies. The shaft total length was 1.524 m, supported on two deep-groove ball bearings 1.357 m apart. Total shaft weight was 155.4 N without the spline sleeve installed and 222.4 N with the sleeve installed. The shaft diameter outboard of the splines was 37.34 mm, while the center section between the two splines was 29.97 mm in diameter and 57.15 mm in length. The active length of each shaft external spline was 38.1 mm while the spline sleeve active length was 133.4 mm in order to span both of the shaft external splines. A close-up of the axial spline coupling is shown in Figure 3. Both shaft splines were identical but were machined $0^{\circ} 18'$ ($\pm 15''$) offset from each other. The static torque preload that resulted was approximately 678 N-m. This torque value is representative of the SSME HPOTP preburner spline. The two shaft splines and the mating internal spline sleeve were fabricated according to the following criteria:

| | |
|-----------------|----------------------|
| Type | Fillet root side fit |
| Number of Teeth | 42 |
| Pressure Angle | 30° |
| Pitch | 20/40 |
| Pitch Diameter | 53.3 mm |
| Base Diameter | 46.1937 mm |
| Surface Finish | 32√ |
| Coating | MoS ₂ |

Kulite ADP-350-300 semiconductor strain gages and specially fabricated high-resolution capacitance displacement probes were used to measure the bending moments and angular displacements, respectively. Four pairs of strain gages were installed on the shaft surface at two axial locations (see Figure 3). At each location, one pair of strain gages was located at $0^\circ/180^\circ$ with respect to the key phase, and another pair was located at $90^\circ/270^\circ$. Eight capacitance probes were installed to measure the angular deflection of the shaft and spline sleeve at four axial locations, where a disc was attached to each end of the spline sleeve and two discs were attached to the shaft outboard of the spline sleeve. At these four axial planes, axial motion was measured in line with the shaker stinger and at 90° to the stinger, and was converted to the angular deflections of that plane. In all cases, precise angular position of the instrumentation is required to ensure the integrity of the data. Circumferential alignment of the bending moment strain gage bridges was maintained to within 0.125° . Likewise, the angular deflection capacitance probes were positioned to the same accuracy from the shaft centerline plane. In addition to the bending moment and angular deflection instrumentation, shaft lateral motion in two orthogonal directions, input force, and acceleration of the input force ram head were measured. While the testing discussed herein relates to nonrotating testing, the instrumentation setup is capable of being used as the shaft is rotated and excited nonsynchronously by the shaker [11].

As shown in Figure 2, the data was acquired by a computer digital data acquisition system. For each test condition, the input force, input acceleration, frequency, shaft motions, axial capacitance probe displacements, and bending moments were measured. To ensure a clear reference signal for all of the data, the oscillator used to drive the MTS hydraulic actuator was run through a synchronous tracking filter and subsequently converted to a square wave signal with a sharp leading edge. This square wave signal was then used as the reference excitation timing signal for all data acquisition.

Prior to conducting the shaker testing, system qualification included a series of low-frequency tests where hysteresis loops of the input strain were plotted against the bending moment beneath the spline sleeve [11]. Once the data instrumentation was qualified, a series of tests was run to acquire bending moment and spline angular deflection data. During the test, data was taken with the shaft oriented so that the $0^\circ/180^\circ$ strain gage pair was directly in line with the shaker stinger. Then, the orientation of the shaft was rotated so that the $90^\circ/270^\circ$ strain gage pair was in line with the stinger, the data was retaken under the same conditions. During the data taking, the off-axis (orthogonal to the stinger plane) bending strain gage data was reviewed and the system alignment was adjusted by rotating the orientation of the shaft manually 1° or 2° to minimize the magnitude of the signal in that plane. Once the out-of-plane bending strain signal was minimized, it was judged that the system was properly aligned.

DATA REDUCTION PROCEDURES

A multi-level rotordynamics model of the test system was developed for a finite-element-based, steady-state linear rotordynamics computer program [12]. The main shaft was divided into 41 elements, and each element was connected by two stations. The axial spline sleeve was modeled as the second level and had 13 elements. The connections between the main shaft and spline sleeve were modeled as two identical bearings. Figure 3 defines the station numbers in this region and shows the locations where the instruments were installed. Each bearing was assumed to have non-zero lateral stiffness, angular stiffness and angular damping, but with zero lateral damping. To simplify the test data reduction procedures, all stiffness and damping were assumed isotropic, and cross-coupling terms were neglected. Introducing anisotropic terms would lead the dynamic

coefficients to be time dependent [10]. Lateral stiffness value was determined by a model developed earlier [9]. The rotordynamics model was tuned to match natural frequencies and mode shapes obtained during impact tests as closed as possible [10].

In the linear rotordynamics computer program, the change in the bending moments, ΔM , and angular deflections, $\Delta\phi$, across the axial spline can be represented by the following equation in terms of the angular stiffness, K_A , and equivalent viscous damping coefficient, B_A [6].

$$\Delta M_i = K_A \Delta\phi_i + B_A \dot{\Delta\phi}_i, \quad i = x, y \quad (1)$$

Physically, it is very difficult to measure the bending moments and angular deflections at the spline coupling locations (stations 25 and 61). Therefore, to approximate the bending moments and angular deflections between stations 25 and 61 (61-25), the original test procedure called for subtracting the bending moments at stations 23 from the bending moment at station 29 (29-23) to arrive at an approximation of the bending moment at the spline coupling. Similarly, the angular deflection at the spline coupling was determined by subtracting the angular deflection at station 30 from that at station 65 (65-30). The initial approximated angular stiffness and damping coefficients were computed by Equation (1). Then, the bending moments and angular deflections at those stations were calculated by the rotordynamics computer program based on the approximated coefficients. An iterative procedure was developed to use both the rotordynamics computer program and Equation (1) interactively until results of the coefficients converged.

Table 1 displays the calculated relative bending moments and angular deflections, both amplitudes and phases, across the spline coupling, stations 61-25, and at the locations to be measured, stations 29-23 and 65-30, for a wide range of angular stiffness and damping coefficients as the shaft was shaking with 222 N at 50 Hz. We found that the coefficients were very sensitive to the accuracy of the phase of the relative angular deflection to be measured. The same phenomenon was found at a lower frequency. This is due to the fact that the shaft is much easier to bend near the outboard of the spline; therefore, the angular deflection of the shaft changes dramatically from station 25 to station 30 (see Figure 4). At the same time, the spline sleeve responded like a rigid body, and the angular deflections of the spline sleeve had almost the same values at both stations 61 and 65. Unfortunately, the change of the shaft angular deflection compensated for the change of the angular deflection across the spline coupling caused by the damping, especially the phase. Therefore, an alternative data reduction procedure was required to determine the dynamic coefficients.

Table 2 shows the calculated absolute bending moments and angular deflections, both amplitudes and phases, at stations 23, 29, 30 and 65, for the same range of angular stiffness and damping coefficients as shown on Table 1, but with an applied load of 222 N at 5 Hz. We found that the absolute amplitude of the bending moment at station 23, the neck section between two splines, decreased as the angular stiffness increased, and the phase, with respect to the phase of a key location, of the bending moment at station 23 increased as the damping decreased. As the frequency increased, the amount of the change in both amplitude and phase due to the change in angular stiffness and damping increased. The amount of change was both measurable and distinguishable, providing an opportunity to use only the bending moment at station 23 to determine the angular stiffness and equivalent viscous damping coefficient. Other measured data act as checking points against which to compare the calculated data.

The revised data reduction procedure is: (i) measure the bending moments at both stations 23 and 29, and angular deflections at both stations 30 and 65; (ii) calculate these bending moments and

angular deflections by a rotordynamics computer program based on guessing values of K_A and B_A ; (iii) adjust K_A and B_A until the amplitude and phase of the bending moment at station 23 match the measured data; (iv) perform minor adjustment of K_A and B_A to minimize the sum of the relative errors due to the difference between the calculated and measured data at stations 29, 30 and 65.

RESULTS AND DISCUSSION

The tests were conducted at three levels of external shaking forces: 80.4, 162.6, and 221.1 N at 5 Hz while the shaft was not rotated. At each force level, three data sets were taken, and we found that the variations of all measured data were within 1% in amplitude and 0.2° in phase. As the orientation of the shaft was rotated 90° , the same accuracy was achieved.

Table 3 displays the calculated angular stiffness and damping coefficients of the three force levels using the revised data reduction procedures. The comparisons of the measured data and predicted values at those four stations are also shown in the same table. For all three force levels, the errors between measured data and predicted values are all within 5%. However, we expect that the errors may increase as the shaking force frequency increases.

Note that for these three test cases, the angular stiffness decreases and damping increases as the force increases. This may be due to the fact that the relative motion between contact surfaces of the spline and sleeve increases as the shaking force increases. To determine the source and the mechanism of damping of the spline coupling, more studies are required, especially testing at different static preload torque levels of the spline coupling; however, this requires a permanent change of the hardware.

The sensitivity analyses were performed for the case with 222 N shaking force at 5 Hz to study the effects of the accuracy of both the rotordynamics model as well as the measured geometrical configurations. On Table 4, which shows the results of the sensitivity analyses, it can be seen that the values of the various parameters were changed somewhat from the baseline values. The change occurred in ball bearing stiffness, K_B ; spline lateral stiffness, K_R ; the shaft diameters, D_{23} and D_{29} , at station 23 and 29, respectively; the length between two splines, L_{22-24} ; the installed bending strain gage locations at both station 23 and station 29; the orientation of the shaft, ϕ_{Key} ; and the misalignment of the external shaking force stinger. We found that all the parameters have little effect on the accuracy of predicting bending moments and angular deflections at stations 23, 29, 30 and 65. The biggest error is caused by the misalignment of the orientation of the shaft; however, in our experiment, we were able to reduce the misalignment to within 2° . After the sensitivity analyses were performed, we were able to conclude that the accuracy of the angular stiffness and damping coefficient determination relied on the accuracy of the measured amplitudes and phases at all four stations, but was unaffected by the revised data reduction procedures.

CONCLUSIONS

A unique test methodology and data reduction procedures were developed in order to measure the bending moments and angular deflections transmitted across an axial spline coupling while the nonrotating shaft was excited by an external shaker. The angular stiffness and equivalent viscous damping coefficients were determined by the interactive use of rotordynamics computer program simulations and experimental measurements. Sensitivity analyses were performed to demonstrate that the proposed data reduction procedure has little effect on the accuracy of the results.

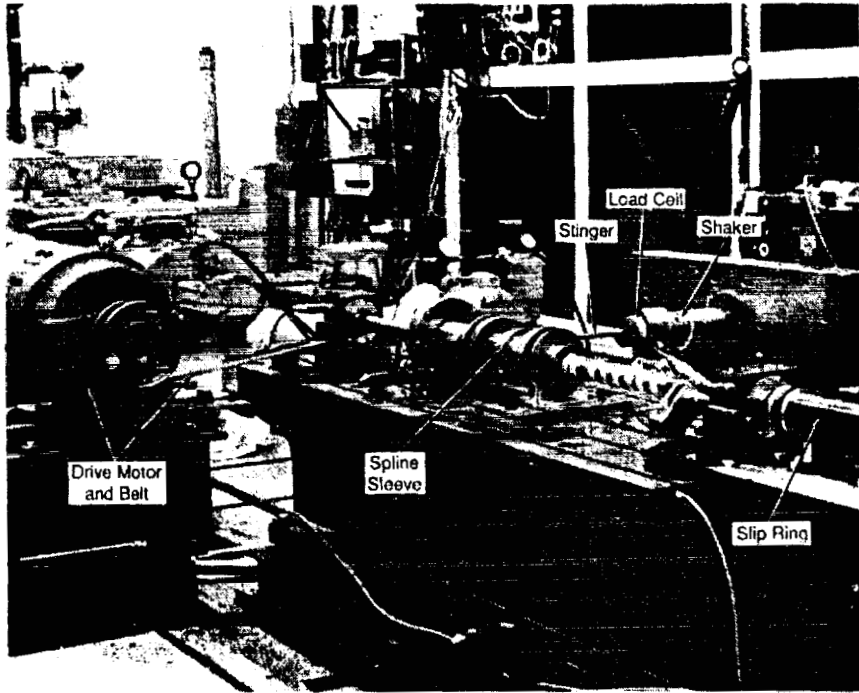
For the three shaking force levels tested at 5 Hz, the errors between the measured data and the predicted values are all within 5%. In addition, we found that for these three test cases the angular stiffness decreases and damping increases as the force increases. However, more tests are required to determine the source and the mechanism of damping of the spline coupling, such as the measurements for different static preload torque levels of the spline coupling.

ACKNOWLEDGMENTS

The authors express their appreciation to the NASA Marshall Space Flight Center, the principal supporter of the work reported in this paper, for their generous support. The authors would also like to thank Messrs. D. Buesing, L. Hoogenboom, P. Quantock, and D. Smith of Mechanical Technology Incorporated for their help in preparing the test facilities.

REFERENCES

1. Newkirk, B. L., 1924, "Shaft Whipping," *General Electric Review*, Vol. 27, No. 3, March, pp. 169-178.
2. Kimball, A. L. Jr., 1924, "Internal Friction Theory of Shaft Whirling," *General Electric Review*, Vol. 27, No. 4, April, pp. 244-251.
3. Robertson, D., 1935, "Hysteretic Influences on The Whirling of Rotors," *Proc. of Inst. Mech. Engr.*, Vol. 131, pp. 513-537.
4. Gunter, E. J. Jr., 1967, "The Influence of Internal Friction on The Stability of High Speed Rotors," *ASME, J. of Engineering for Industry*, Vol. 89, No. 4, pp. 683-688.
5. Williams, R. Jr., and Trent, R., 1970, "The Effects of Nonlinear Asymmetric Supports on Turbine Engine Rotor Stability," *SAE 700320*.
6. Lund, J. W., 1986, "Destabilization of Rotors from Friction in Internal Joints with Micro-Slip," *Proc. of The International Conference on Rotordynamics*, September 14-17, Tokyo, pp. 487-491.
7. Bannister, R. H., 1980, "Methods for Modeling Flanged and Curvic Couplings for Dynamic Analysis of Complex Rotor Constructions," *ASME, J. of Mechanical Design*, Vol. 102, No. 1, pp. 130-139.
8. Marmol, R. A., Smalley, A. J., and Tecza, J. A., 1980, "Spline Coupling Induced Nonsynchronous Rotor Vibrations," *ASME, J. of Mechanical Design*, Vol. 102, No. 1, pp. 168-176.
9. Walton, J. F. Jr., Artiles, A., Lund, J. W., Dill J., and Zorzi, E., 1990, "Internal Rotor Friction Instability," *Mechanical Technology Incorporated, Latham, New York, 88TR39*.
10. Ku, C.-P. R., Walton, J. F. Jr., and Lund, J. W., 1993, "A Theoretical Approach to Determine Angular Stiffness and Damping Coefficients of An Axial Spline Coupling in High Speed Rotating Machinery," submitted to the 14th Biennial Conference on Mechanical Vibration and Noise, September 19-22, Albuquerque, New Mexico.
11. Walton, J. F. Jr., Ku, C.-P. R., and Lund, J. W., 1993, "An Experimental Investigation of the Dynamic Characteristics of An Axial Spline Coupling in High Speed Rotating Machinery," submitted to the 14th Biennial Conference on Mechanical Vibration and Noise, September 19-22, Albuquerque, New Mexico.
12. Tecza, J. A., Malanoski, S. B., and Ku, C.-P. R., 1991, Rotordynamics and Modeling Workshop, Electric Power Research Institute, Eddystone, Pennsylvania, June 4-6.



V93-51

Figure 1 Experimental setup.

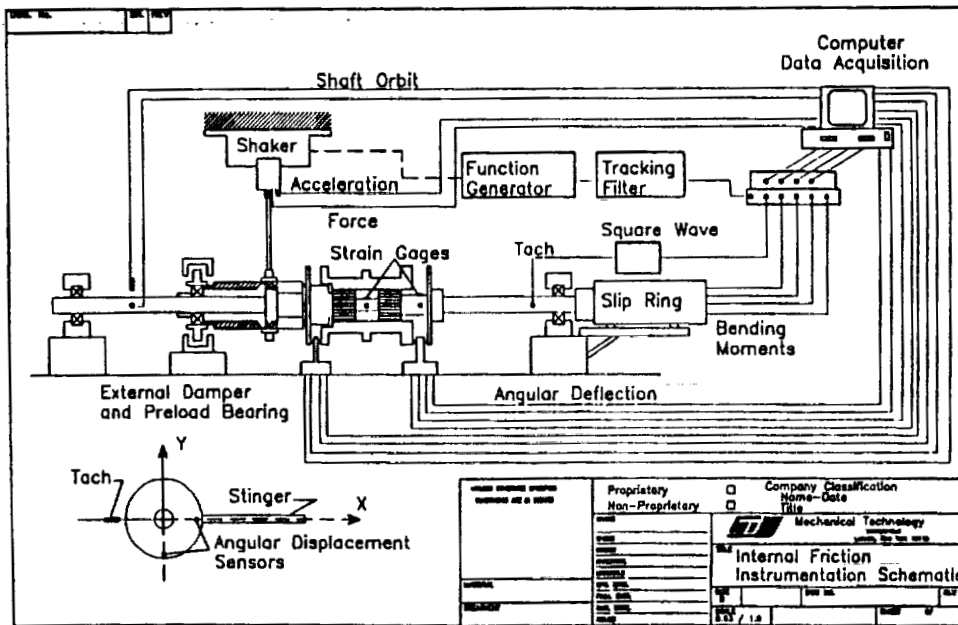


Figure 2 Experimental test setup functional diagram.

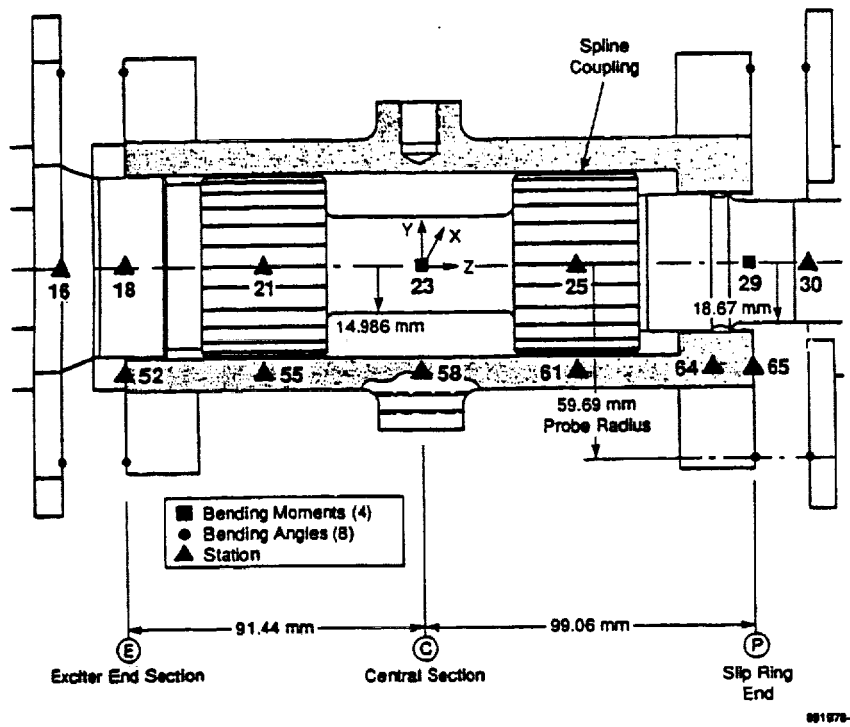


Figure 3 Close-up of the axial spline coupling and instrumentation installed locations

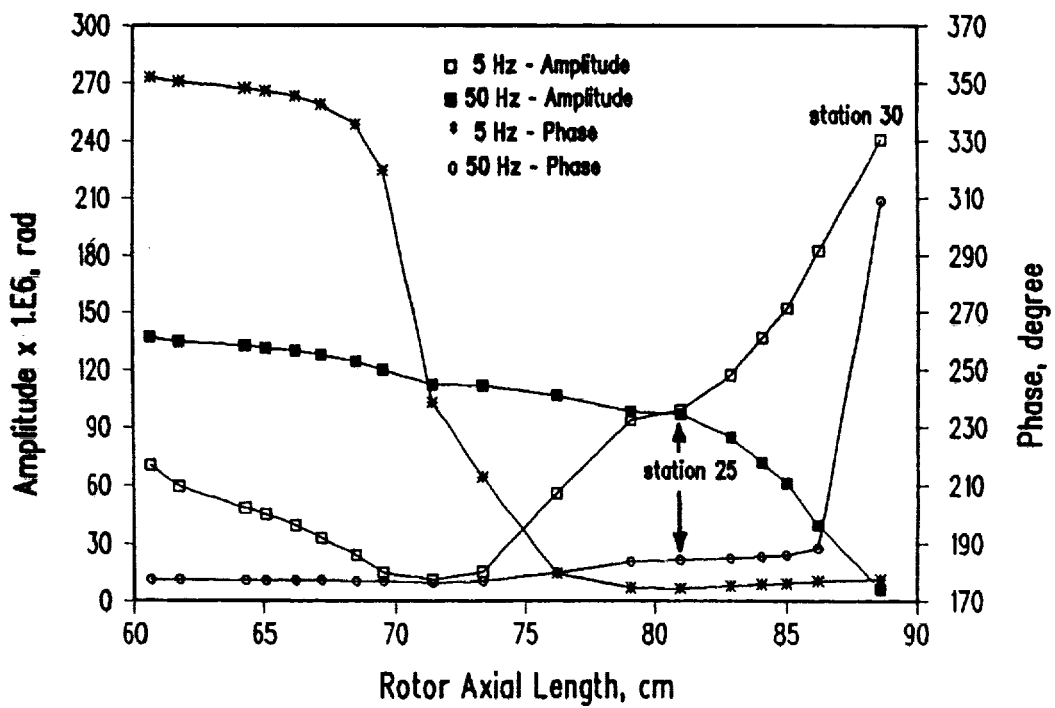


Figure 4 Predicted angular displacements at 225 N external force ($K_A=1.13 \times 10^6$ N-m/rad, $B_A=1.13 \times 10^4$ N-m-s/rad)

Table 1 Predicted relative bending moments and angular deflections
(222 N horizontal external shaking force at 50 Hz)

| K _A | B _A | M _y (29-23) | | M _y (61-25) | | φ _y (65-30) | | φ _y (61-25) | |
|----------------|----------------|------------------------|-------|------------------------|-------|------------------------|-------|------------------------|-------|
| | | Amp. | Phase | Amp. | Phase | Amp. | Phase | Amp. | Phase |
| N-m/rad | N-m-s/rad | N-m | deg. | N-m | deg. | rad | deg. | rad | deg. |
| 1.13E6 | 1.13E2 | 27.89 | 0.4 | 25.78 | 0.5 | 1.167E-4 | -0.2 | 2.281E-5 | -1.3 |
| | 1.13E3 | 28.36 | 3.7 | 26.32 | 4.4 | 1.160E-4 | -1.6 | 2.223E-5 | -13.0 |
| | 1.13E4 | 34.94 | 4.9 | 33.78 | 5.8 | 1.046E-4 | -2.9 | 0.907E-5 | -66.6 |
| 1.13E7 | 1.13E2 | 35.03 | 0.0 | 33.85 | 0.0 | 1.040E-4 | 0.0 | 2.997E-6 | -0.2 |
| | 1.13E3 | 35.03 | 0.1 | 33.85 | 0.1 | 1.040E-4 | 0.0 | 2.995E-6 | -1.7 |
| | 1.13E4 | 35.12 | 0.5 | 33.96 | 0.6 | 1.039E-4 | -0.3 | 2.868E-6 | -16.9 |
| | 1.13E5 | 35.99 | 0.5 | 34.96 | 0.6 | 1.023E-4 | -0.3 | 0.939E-6 | -71.7 |
| 1.13E8 | 1.13E2 | 35.99 | 0.0 | 34.95 | 0.0 | 1.023E-4 | 0.0 | 3.094E-7 | 0.0 |
| | 1.13E3 | 35.99 | 0.0 | 34.95 | 0.0 | 1.023E-4 | 0.0 | 3.094E-7 | -0.2 |
| | 1.13E4 | 35.99 | 0.0 | 34.95 | 0.0 | 1.023E-4 | 0.0 | 3.093E-7 | -1.8 |
| | 1.13E5 | 35.99 | 0.1 | 34.96 | 0.1 | 1.023E-4 | 0.0 | 2.953E-7 | -18.4 |

Table 2 Predicted absolute bending moments and angular deflections
(222 N horizontal external shaking force at 5 Hz)

| K _A | B _A | M _y (23) | | M _y (29) | | φ _y (30) | | φ _y (65) | |
|----------------|----------------|---------------------|-------|---------------------|-------|---------------------|-------|---------------------|-------|
| | | Amp. | Phase | Amp. | Phase | Amp. | Phase | Amp. | Phase |
| N-m/rad | N-m-s/rad | N-m | deg. | N-m | deg. | rad | deg.* | rad | deg.* |
| 1.13E6 | 1.13E2 | 12.78 | -0.1 | 51.45 | 0.0 | 2.434E-4 | 0.0 | 6.097E-5 | 0.0 |
| | 1.13E3 | 12.78 | -0.2 | 51.45 | 0.0 | 2.434E-4 | -0.2 | 6.098E-5 | 0.0 |
| | 1.13E4 | 12.40 | -11.8 | 51.44 | 0.0 | 2.411E-4 | -2.3 | 6.102E-5 | 0.1 |
| 1.13E7 | 1.13E2 | 3.51 | 0.0 | 51.34 | 0.0 | 2.077E-4 | 0.0 | 6.117E-5 | 0.0 |
| | 1.13E3 | 3.51 | -0.1 | 51.34 | 0.0 | 2.077E-4 | 0.0 | 6.117E-5 | 0.0 |
| | 1.13E4 | 3.51 | -0.6 | 51.34 | 0.0 | 2.077E-4 | 0.0 | 6.117E-5 | 0.0 |
| | 1.13E5 | 3.42 | -5.9 | 51.34 | 0.0 | 2.073E-4 | -0.4 | 6.117E-5 | 0.0 |
| 1.13E8 | 1.13E2 | 2.38 | 0.0 | 51.32 | 0.0 | 2.033E-4 | 0.0 | 6.116E-5 | 0.0 |
| | 1.13E3 | 2.38 | 0.0 | 51.32 | 0.0 | 2.033E-4 | 0.0 | 6.116E-5 | 0.0 |
| | 1.13E4 | 2.38 | 0.0 | 51.32 | 0.0 | 2.033E-4 | 0.0 | 6.116E-5 | 0.0 |
| | 1.13E5 | 2.38 | -0.1 | 51.32 | 0.0 | 2.033E-4 | 0.0 | 6.116E-5 | 0.0 |

* With respect to 180°

Table 3 Test cases with horizontal external shaking force at 5 Hz

| | Unit | F=80.4 N* | F=162.6 N* | F=221.1 N* |
|------------------------------|---------------------|---------------------------|---------------------------|---------------------------|
| K_A - calculated | N-m/rad | 2.79 E6 | 2.52 E6 | 2.31 E6 |
| B_A - calculated | N-m-s/rad | 3.7 E3 | 6.0 E3 | 6.9 E3 |
| $M_Y(29)$ - measured | N-m | 19.10 | 38.61 | 52.58 |
| $M_Y(29)$ - calculated | N-m | 18.58 (2.7%) [§] | 37.61 (2.6%) [§] | 51.13 (2.8%) [§] |
| $M_Y(23)$ - measured | N-m | 2.83 | 6.06 | 8.71 |
| $M_Y(23)$ - calculated | N-m | 2.75 (2.8%) [§] | 5.90 (2.7%) [§] | 8.46 (2.8%) [§] |
| $M_X(29)$ - measured | N-m | 0.39 (2.0%) [@] | 0.75 (1.9%) [@] | 1.59 (3.0%) [@] |
| $M_X(29)$ - calculated | N-m | 0 | 0 | 0 |
| $M_X(23)$ - measured | N-m | 0.07 (2.5%) [@] | 0.18 (3.0%) [@] | 0.09 (1.1%) [@] |
| $M_X(23)$ - calculated | N-m | 0 | 0 | 0 |
| $M_Y(23)$ phase - measured | degree [#] | -1.43 | -2.6 | -3.2 |
| $M_Y(23)$ phase - calculated | degree [#] | -1.4 | -2.6 | -3.2 |
| $\phi_Y(30)$ - measured | μm | 4.72 | 9.58 | 13.18 |
| $\phi_Y(30)$ - calculated | μm | 4.78 (1.1%) [§] | 9.73 (1.6%) [§] | 13.31 (1.0%) [§] |
| $\phi_Y(65)$ - measured | μm | 1.30 | 2.59 | 3.48 |
| $\phi_Y(65)$ - calculated | μm | 1.32 (2.0%) [§] | 2.67 (2.9%) [§] | 3.63 (4.4%) [§] |

* Data are average of 3 test cases, the deviations are: amplitude ($\pm 1\%$), phase ($\pm 0.2^\circ$)

With respect to $M_Y(29)$

§ Relative error with respect to measured data

@ Relative error with respect to measured data at M_Y

Table 4 Sensitivity analyses of 222 N horizontal external shaking force at 5 Hz

| | $M_y(23)$ | | $M_x(23)$ | $M_y(29)$ | $M_x(29)$ | $\phi_y(30)$ | $\phi_x(30)$ | $\phi_y(65)$ | $\phi_x(65)$ |
|---------------------------------|-----------|---------------|-----------|-----------|-----------|--------------|--------------|--------------|--------------|
| | Amp. | Phase | Amp. | Amp. | Amp. | Amp. | Amp. | Amp. | Amp. |
| $K_B=1.75E7$ N/m | 0.01% | --- | --- | 0.07% | --- | 0.8% | --- | 3% | --- |
| $K_R \pm 7.01E8$ N/m | --- | --- | --- | --- | --- | --- | --- | 0.3% | --- |
| $D_{23} \pm 0.51$ mm | 5% | --- | --- | --- | --- | 0.1% | --- | 0.1% | --- |
| $L_{22-24} \pm 0.25$ mm | 0.3% | --- | --- | --- | --- | --- | --- | --- | --- |
| $D_{29} \pm 0.51$ mm | 0.01% | --- | --- | 0.02% | --- | 1% | --- | 3% | --- |
| M_{23} location ± 2.5 mm | 1.3% | 0.03° | --- | --- | --- | --- | --- | --- | --- |
| M_{29} location ± 2.5 mm | --- | --- | --- | 0.4% | --- | --- | --- | --- | --- |
| $\phi_{Key} \pm 5^\circ$ # | 0.4% | --- | 8.7% | 0.4% | 8.7% | 0.4% | 8.7% | 0.4% | 8.7% |
| Force Misalignment ± 2.5 mm | 0.01% | --- | --- | --- | --- | --- | --- | --- | --- |
| Combination | 7% | $< 0.1^\circ$ | 8.2% | 0.1% | 8.8% | 0.6% | 8.7% | 6% | 9.3% |

The base line case uses the following parameters: $K_A=2.03E6$, $B_A=5.65E3$, $K_B=1.23E8$, $K_R=1.21E8$,

$D_{23}=29.97$ mm, $D_{29}=37.34$ mm, $L_{22-24}=57.15$ mm, $\phi_{Key}=0^\circ$

Experiment is able to reduce the misalignment of the orientation of the shaft to within 2°